New methodology for flight control system sizing and hinge moment estimation

Original Article

Institution of MECHANICAL ENGINEERS
Journal of AEROSPACE ENGINEERING

Proc IMechE Part G:
J Aerospace Engineering
2021, Vol. 0(0) 1–16

DOI: 10.1177/09544100211063110
journals.sagepub.com/home/pig
SAGE

New methodology for flight control system sizing and hinge moment estimation

Carlos Cabaleiro de la Hoz[1] and **Marco Fioriti**[2]

Abstract

Flight control surfaces guarantee a safe and precise control of the aircraft. As a result, hinge moments are generated. These moments need to be estimated in order to properly size the aircraft actuators. Control surfaces include the ailerons, rudder, elevator, flaps, slats, and spoilers, and they are moved by electric or hydraulic actuators. Actuator sizing is the key when comparing different flight control system architectures. This fact becomes even more important when developing more-electric aircraft. Hinge moments need to be estimated so that the actuators can be properly sized and their effects on the overall aircraft design are measured. Hinge moments are difficult to estimate on the early stages of the design process due to the large number of required input. Detailed information about the airfoil, wing surfaces, control surfaces, and actuators is needed but yet not known on early design phases. The objective of this paper is to propose a new methodology for flight control system sizing, including mass and power estimation. A surrogate model for the hinge moment estimation is also proposed and used. The main advantage of this new methodology is that all the components and actuators can be properly sized instead of just having overall system results. The whole system can now be sized more in detail during the preliminary design process, which allows to have a more reliable estimation and to perform systems installation analysis. Results show a reliable system mass estimation similar to the results obtained with other known methods and also providing the weight for each component individually.

Keywords

flight control system, hinge moment, more electric aircraft

Date received: 16 April 2021; accepted: 9 November 2021

Introduction

Aircraft control is achieved by the flight control system (FCS). This is one of the main subsystems of the aircraft and it is constituted of the control surfaces, actuators, commands, and flight control computers, although these last ones can also be counted as part of the avionics. The pilot acts on the different commands (i.e., stick and pedals) to control the maneuvres. Some aircraft do not have digital flight control systems and the required forces are generated through a mechanical chain between the pilot commands and the control surfaces. Regarding digital FCS, the pilot commands altogether with the flight control computers which create a signal to activate the actuators. These actuators deflect the control surfaces, and as a result, the required forces are generated. The joint line between control surfaces and actuators is called hinge line. Hinge moments and forces are generated when these surfaces are deflected; hence, they define the requirements for the actuators.

Control surfaces are divided into primary and secondary. Primary surfaces (i.e., rudder, ailerons, and elevator) are used to control the attitude of the aircraft around the three control axes: pitch, roll, and yaw. They are constantly active during flight. Secondary control surfaces (i.e., flaps, slats, and spoilers) are only used in some specific segments of the mission profile (e.g., landing and take-off) and their main function is to modify the wing geometry to increase lift and/or drag during that specific segment.

Actuators can be rotary or linear. Depending on their power source, they can be electric, hydraulic, or a combination of both.

The current tendency on the industry is to increase the electrification level of the aircraft due to its potential advantages. This trend is called "more electric aircraft (MEA)." Replacing hydraulic components with electrical ones might reduce the overall weight of the aircraft and

[1] Research Engineer, Mechanical and Aerospace Engineering Department, Politecnico di Torino, Turin, Italy
[2] Assistant Professor, Mechanical and Aerospace Engineering Department, Politecnico di Torino, Turin, Italy

Corresponding author:
Marco Fioriti, Department of Mechanical and Aerospace Engineering, Politecnico di Torino, C.so Duca degli Abruzzi n.24, Turin, 10100, Italy.
Email:marco.fioriti@polito.it

might also have a positive impact on maintenance.[1] This trend also applies specifically to the FCS, and as a result, more-electric actuators are substituting the classic hydraulic ones.[1,2] The main penalties of hydraulic circuits reside on the hydraulic system weight while electric components can potentially reach lighter overall subsystems' weight by removing it.[3] Electric actuators usually require a higher engine off-takes power extraction, which penalizes the fuel consumption.[4] Actuators need to be sized in order to be able to evaluate this trade-off. As a result, hinge moment estimation becomes an important analysis.

The main types of actuators used on aviation are now summarized[5]:

- Conventional hydraulic servo actuator (HSA): It is powered by redundant hydraulic supply lines. These are heavy and add lots of subsystems from the pumps to the actuators.
- Electro-hydrostatic actuator (EHA): It is also hydraulic but each actuator has its own local hydraulic circuit that is given power by an electrically driven motor.[6] Central hydraulic unit is substituted by a local hydraulic system for the actuator.
- Electric backup hydraulic actuator (EBHA): It consists of a HSA actuator with a second hydraulic supply line like in the EHA. In normal operation, the central hydraulic line is moving the actuator, and in case of failure (backup mode), the local unit drives the hydraulics. Hence, redundancies reside on the actuator and not on the supply line.
- Electro-mechanical actuator (EMA): It replaces electro hydraulic powering from the EHA with an electric motor and a gearbox assembly.

Some FCS architecture examples are now given to the reader for a better understanding. In A320, all actuators are hydraulic (HSA) supplied by three different hydraulic lines.[7] For A380, some EHA and EBHA actuators were implemented achieving a higher level of electrification.[8] Continuing the MEA tendency, the A350 model used both EHA and EMA actuators, and as a result, one of the three hydraulic lines was removed and substituted by electric ones.[9]

Hinge moment estimation is the key when a subsystem level design is required. The importance of knowing the hinge moment is now highlighted. It is needed for

- actuators sizing;
- flight control system mass and required power estimation;
- hydraulic and electric systems sizing;
- estimating the differences between conventional and more-electric architectures; and
- calculating the off-takes impact on the engine's performance.

Hinge moments can be estimated in several ways depending on the fidelity level required. Higher-fidelity models are performed with computational fluid dynamics (CFD). Two-dimensional numerical aerodynamic models can also be used, but they do not provide accurate results as expected.[10] For preliminary design, Roskam's method could be the best option in terms of fidelity and computational time. In particular, this calculation method can be found in detail on reference.[11] Only the elevator, rudder, and ailerons can be modeled with this method though. Flaps, slats, and spoilers require another model that will be commented later.

Other important issue to be taken into consideration is the type of actuator used on each device. Ailerons, rudders, elevators, and spoilers are usually moved by classic linear actuators while flaps and slats have ball-screw ones. Actuation times are different, while flaps and slats are deployed in tens of seconds that the other control surfaces must act in much lower times close to seconds. As a result, primary control surfaces and spoilers generate a hinge moment that has to be compensated by the linear actuators. Flaps and slats generate a hinge force that is counteracted by the ball-screw actuators.

The main problem with Roskam's approach is that the input needs a high level of detail that is not achieved on early stage design phases. Some of the input values include

- altitude, angle of attack and slip, the Mach number, and control surface deflections on each of the mission profile segments;
- all the geometric parameters to define the wing, vertical, and horizontal tail;
- each of the control surfaces' position, chord, profile, geometry, nose shape, and gap; and
- the hinge moment coefficient for null angle of attack for each airfoil, calculated experimentally.

As it can be seen, some of these values are not defined on a preliminary analysis. Here resides the need of developing a surrogate model.

Hinge moments are not usually found or shared. Their estimation can be difficult and industry does not generally publish the values. Some universities have published some research as an attempt to provide some reference values to the public.[10–13] In general, Roskam and CFD are the most used methods, but there are also some cases in which researchers develop their own methods based on these previous analyses.[14] In general, hinge moments exact values are not provided and only estimations and approaches are to be found.[15,16]

Another way of estimation for reference or model calibration is doing reverse engineering. Actuators stall load (i.e., output force) and nominal stroke can sometimes be found. Hence, the maximum hinge moment can be estimated knowing which actuator is used by which control surface. The moment arm is deduced with the nominal stroke, and the maximum deflection angle and the force is obtained from the actuator's stall load and a safety margin. Hence, a reliable prediction of the elevator's,

rudder's, and ailerons' hinge forces might be done with this information.

Regarding the flaps and slats, as commented before, the kinematic chain formed by the actuator, bars, and hinges has some influence in the results. In general, this kinematic chain architecture is assumed and simplified in order to have quick values. They can also be obtained from experimental data.[14]

Spoilers are also tough to calculate. This resides on the high deflection angles and their position on the middle of the wing and not on the leading or trailing edge. Flight spoilers are active during flight, and deflections are lower but Mach numbers are high. Ground spoilers are deployed during landing. On this case, the speed is low but the deflection angles are huge.[17,18] A simplified model is proposed by modeling them as a flat plate.[19]

Some information about components' mass can be found in literature. Most of them give estimations for different actuators and components,[3,20,21] but there is not a unified model for all of them.

The main technical contribution of this paper is the capability to size the whole flight control system at a component at early stages of the project when the detailed input that the hinge moment estimation requires is not known. Besides, the flight control system is needed in order to size the electrical and hydraulic systems, having an impact on the whole on-board systems.

The importance of having a reliable model for hinge moment estimation has been highlighted. The section Methods describes the method that is used in this analysis for each of the aircraft's control surfaces. The results of the surrogate model are shown in the section Hinge Moment Surrogate Model Results. The section Mass and Power Estimation shows how to make the mass and power estimation from the results provided by the hinge moment surrogate model. The section Application Case: A320 FCS Mass Estimation shows an application case on how to use the surrogate model and mass estimation method to calculate the mass of the A320 flight control system, and then it is compared to other methods. The conclusions are summarized in the last section. Nomenclature can be found in the Appendix.

Method

Roskam's method was mainly used for this analysis. This model has some limitations since it considers the following assumptions.

- Subsonic flow is found in all the wings.
- The relation between the plain flap chord c_f and the wing surface chord c should be between 0.1 and 0.4 (Figure 1).
- The maximum gap allowed between wing surface and control surface is 0.5% of the wing's chord length.
- Overhang $[c_b/c_f]$ values shall be between 0.1 and 0.5 (Figure 1).
- High surface deflections are not considered ($\delta > 30°$).
- Airfoil thickness should not surpass values over 20%.

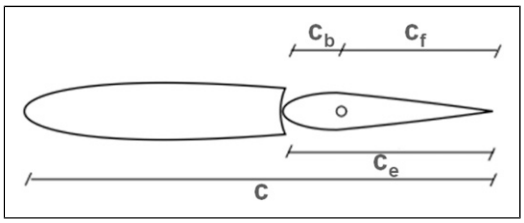

Figure 1. Control surface schema

- Control surfaces' nose shape shall be smooth.

This model fits for the primary control surfaces of conventional civil aircraft so it can be used on this context. Hence, ailerons, rudder, and elevator can be sized using Roskam's approach. Flaps and slats have an important contribution due to the diverse mechanical devices that are involved in their deployment. They cannot be sized by Roskam's method. Depending on which type of high lift device is used, the results may vary. A detailed normal load calculation is done in order to estimate the actuator's forces. Spoilers cannot be sized with Roskam's approach either, so they were modeled as a flat plate. The problem resides on the high spoiler deflection angles that are usually used, the spoiler's thickness, and their position in the wing. The drag coefficient for the spoilers has to be estimated then. Three different methods are needed in order to size all the control surfaces. As a summary, we can point out as follows:

- Roskam's method is used for ailerons, elevator, and rudder.
- The flat plate model is used for the spoilers.
- Normal load calculation is selected for flaps and slats.

The three approaches are implemented in the methodology and are now explained more in-depth. Results are shown in the section Hinge Moment Surrogate Model Results.

Input

A list of all the involved inputs is now provided. The number of values needed is huge and needs to be reduced for the surrogate model. First, information about the control surfaces geometry is needed for the two-dimensional estimation of the hinge coefficients for the primary control surfaces. These values include

- c_f/c (Figure 1);
- overhang (c_b/c_f) (Figure 1);
- control surface's nose shape (usually round, elliptic, sharp or a combination of them);
- gap between both surfaces;
- hinge moment coefficient for null angle of attack, experimentally calculated; and
- control surface's airfoil, used to calculate the maximum thickness, hinge thickness, and trailing edge angle.

Information about the wing surfaces (i.e., wing, horizontal tail, and vertical tail) is also needed in order to make the 3-D correction to the hinge moment coefficients. These additional input values include

- wing, horizontal tail, and vertical tail areas;
- wing, horizontal tail, and vertical tail sweep and aspect ratio;
- spoilers, and flap and slat areas; and
- position of each control surface relative to its corresponding wing surface.

Mission profile data is also needed for all the three methods. The following list shows the input values that are needed to be known at each of the mission profile segments:

- Altitude, Mach number, angle of attack and drift angle;
- the control surfaces' (i.e., ailerons, rudder, elevator, flaps, slats, and spoilers) deflection, as well as the maximum values; and
- trimmable horizontal stabilizer and downwash angles.

Hinge Moment Coefficients (Primary Control Surfaces)

The main equation of Roskam's method is shown in equation (1) for a better understanding of the model. Reference 11 provides a detailed explanation of the procedure. Summarizing, it specifies how to estimate the two-dimensional coefficients and then sum them. The procedure includes some regressions taken from experimental data. The main parameters that affect the hinge moment coefficients are now shown

$$C_h = C_{h_0} + C_{h_\alpha} \cdot \alpha + C_{h_\delta} \cdot \delta + C_{h_{\delta_t}} \cdot \delta_t \quad (1)$$

Equation (1) is now explained in detail. It calculates the hinge moment coefficient of a generic control surface as a function of the angle of attack (α), the angle of deflection (δ), and the tab deflection (δ_t). The first component (C_{h_0}) is the zero angle of attack, zero control surface deflection, and zero tab-angle-deflection hinge moment coefficient. It is null for symmetrical airfoils. Experimental data should be used for cambered ones. Since experimental values are not generally known, those proposed by Roskam were taken for the method. The second component (C_{h_α}) is the control surface hinge moment derivative due to the angle of attack. It depends on the airfoil's shape and thickness, overhang, the relation between plain flap chord and control surface chord, and the two-dimensional lift coefficients. It is then corrected by the nose shape, gap, and Mach effect. The third component (C_{h_δ}) is the control surface hinge moment derivative due to control surface deflection. It depends on the airfoil's shape and thickness, airfoil's hinge-point thickness, overhang, the relation between plain flap chord and control surface chord, and the two-dimensional lift coefficients as well as the previous coefficient, it is corrected by the nose shape, gap, and Mach effect. The fourth component $(C_{h_{\delta_t}})$ is the control surface hinge moment derivative due to a tab deflection. Since information about tab characteristics was not found, this effect was not taken into consideration. After these 2-D coefficients are calculated following Roskam's instructions,[11] some corrections are made in order to consider 3-D effects induced by the wing and tail surfaces. Here, the aspect ratio, and sweep and control surface position values are needed, as well as the hinge-line sweep angle.

The alpha and beta angles are to be known in order to use equation (1), as well as each control surface's deflections δ. They shall be estimated for each mission segment. The mission profile that was considered is formed by six segments, which are take-off, climb, cruise, descent, landing, and high speed maneuvre.

As an example for the reader, the estimation of the deflection angles is shown in Table 1. Knowing the maximum deflection, they can be expressed as a percentage of it. Values on these tables are just an example and may vary from one aircraft to another. It can be seen how the aileron positive and negative deflections differ on some cases; this is due to the adverse yaw issue and the differential aileron deflection solution to it. It can also be seen how during landing the deflections are higher due to the side-wind conditions that the aircraft need to fulfill.

Other values need to be given for the spoilers, flaps, and slats although on these cases they are not active during all the mission profile. Flaps and slats are only active during take-off and landing and ground spoilers only at landing.

Flap deflection can reach values up to 45° on big aircraft, while deflections are lower on smaller ones (around 30°). Slats' angles are a bit lower but can reach around 27° in some cases. Ground spoilers are used to destroy lift and create drag; hence, their deflections can reach really high values like 60° or even more. Each aircraft has different values and they should be studied for each of them.

Hinge moment estimation for primary control surfaces

Once the coefficients have been obtained, the hinge moment can be calculated as the rest of the flight dynamics coefficients

$$M_{hinge} = q \cdot S_w \cdot c \cdot C_h \quad (2)$$

where q is the dynamic pressure, S_w is the wing (or vertical or horizontal tail) surface, c is the surface's standard mean chord, and C_h is the hinge moment coefficient calculated before and mentioned in the section Hinge Moment Coefficients (Primary Control Surfaces).

As explained before, all the mission segments are considered so the dynamic pressure has to be obtained for each of them. This can be easily done since the Mach number and altitude are known from the input.

Table 1. Example of primary control surfaces deflection angles for each mission segment.

	Max	Take-Off	Climb	Cruise	Descent	Landing	Maneuvre
Ailerons	25°	+15/-20%	+15/-20%	+50/-50%	+15/-20%	+40/-53%	+30/-30%
Rudder	30°	+20/-20%	+20/-20%	+30/-30%	+20/-20%	+53/-53%	+30/-30%
Elevator	30°	+20/-20%	+20/-20%	+30/-30%	+20/-20%	+53/-53%	+30/-30%

Hinge moment estimation for spoilers

As said before, hinge moment of the spoilers cannot be calculated using Roskam's method owing to these surfaces' characteristics. Therefore, another approach is needed. The simplest method would be assuming that the spoilers are low-aspect ratio flat plates,[18] for which some experimental data can be found. Thanks to this analysis, some reliable reference values about flat plates are found. The drag coefficient can be estimated, and with it, the spoilers' drag. With the drag value and the force's arm, the total moment on the hinge line is found. Equation (3) is the result from the analysis

$$\mathrm{M}_{hinge} = q \cdot S_{spoiler} \cdot C_{d_{spoiler}} \cdot arm_{spoiler} \tag{3}$$

where q is the dynamic pressure and $S_{spoiler}$ is the spoiler's surface. The arm is known by knowing the spoiler's deflection and chord. The drag coefficient is estimated with experimental data.[19] It is a function of the spoiler's deflection, and it is corrected with the Reynold's number.

This approach can be made for ground spoilers since they are deployed during the landing run. Mach numbers are low and compressibility effects do not have a huge influence. During cruise at close-to-transonic Mach numbers, this method is not valid. On this method, flight spoilers are sized only on landing and not on high speed maneuvres owing to this reason.

Hinge force estimation for flaps and slats

Flaps and slats cannot be modeled with Roskam's approach. The gap between the wing and the surface is bigger than assumed by the method. Also, there is no hinge line since the devices have more complex kinematic chains and mechanisms to connect with the actuators. Hence, the analysis has to be done differently. Equation (4) shows the normal load that the flap is supporting during its deflection

$$\mathrm{N}_f = 1.2 \cdot C_{N_{flap}} \cdot S_{flap} \cdot q \tag{4}$$

where

- 1.2 is the load factor in worst case loading condition.
- $C_{N_{flap}}$ is the normal flap load coefficient. It depends on the flap chord and deflection and the usual values are between 0.9 and 1.2.[22]
- S_{flap} is the flap (or slat) surface.
- q is the dynamic pressure. It is calculated on landing since this is the sizing case (highest deflection).

The actuator load can be estimated once the normal load is obtained. In order to do it, the force needs to be moved from the quarter chord line to the actuator line. The method proposed by Zaccai[23] was used in this analysis. Figure 2 shows some examples of flap mechanisms. As a result, an average value between the values obtained from the dropped hinge and four-bar was used. The whole analysis can be simplified by multiplying equation (4) by a correction factor. The index obtained is usually between 0.6 and 0.8 so a force reduction is achieved. It can be seen that the two suggested flap mechanisms use linear actuators (ball-screw actuator).

Regarding the slats, the same equations can be used. The normal load factor will be lower and the slat mechanism is supposed to be always a dropped hinge. Krueger flaps were not considered since they are sized also with a moment instead of a stall load. Hence, all the leading edges were modeled with simple slat devices.

Model calibration

Two references are used for the calibration of the primary control surfaces and spoiler models: A320 and B737-800. Both have similar weight and characteristics but the main issue resides in that, as said by Peter K. C. Rudolph,[24] hinge moment values can vary up to two or three times more for Boeing aircraft compared to Airbus models. This is due to the fact that they have different hinge positions, mechanisms, and chord relations. Both aircraft's hinge moments are now estimated and compared to check this supposition and then some assumptions are made.

First, Roskam's method is used with the data from B737-800 and compared with the reference values from Ref.14. The results are shown in Table 2. They match for certain values of overhang (i.e., 0.25 for ailerons, 0.3 for rudder, and 0.2 for elevator) and chord relation (i.e., 0.3 for ailerons, 0.3 for rudder, and 0.33 for elevator). Hence, Roskam's approach seems to provide good estimations when the airfoil and surface data are known.

Regarding the A320, the exact values are not known, so in order to have them, some reverse engineering needs to be done. The stroke and stall load values for the A320 actuators are summarized in Table 3. The stall load is the force that the actuator can provide. The stroke is the difference between the maximum and minimum position that the actuator can reach, so it is represented by a length. With the stroke and the maximum and minimum control surface deflection, the moment arm can be estimated by some geometrical relations. This value is also provided in Table 3. With the stall load and moment arm, the reference

hinge moment is obtained. The values calculated with Roskam's method are also shown in order to make a comparison.

The results seem to be precise and appropriate. They were obtained under Roskam's assumptions and limitations but they represent well the control surfaces. The main problem now resides in the difference between Airbus and Boeing results. The biggest difference is obtained in the elevator. An average value between them will be used for the surrogate model.

Another reference is used for validation. A bigger airplane is proposed in order to have distant analysis points. In this case, the studied aircraft is the A330 model. Each of its actuators' stall load can be found in reference 8. Data for the ailerons, elevator, rudder, and spoilers are provided. The obtained values are shown in Table 4 and are called actual stall loads. The estimated hinge moments with Roskam's method for this aircraft are represented on the first line, but notice that the value for the ailerons is divided by two since this aircraft has two ailerons per wing. The deduced arms are calculated from the ones of the A320 multiplied by a scale factor proportional to both wing chords. Hence, the A330 actuators' arms are bigger than those of the A320 and proportional to the chord relation. The estimation of the stall loads can be obtained by dividing the estimated hinge moment and the calculated arm. The values are provided in the last line of Table 4 and are compared with the reference ones. The method seems to represent well the real values having a bigger error on the rudder.

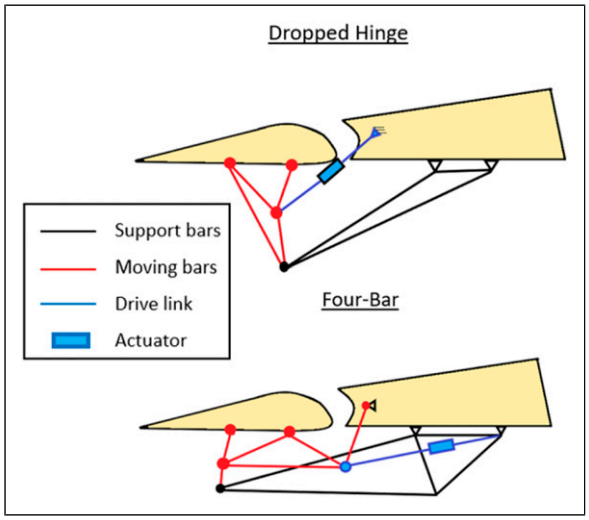

Figure 2. Considered flap mechanisms

Hinge moment surrogate model results

All the proposed aircraft were analyzed with the methodology presented in the section Methods. The objective now is to build the surrogate model. In order to do so, all the results are displayed in graphs trying to find correlations with some of the classic aircraft's most relevant parameters (e.g., wing surface and maximum take-off weight). The list of all the analyzed aircraft is shown in Table 5, in which the airplane names can be seen with some relevant data that would be used afterward for the different correlations. The aircraft have been labeled with

Table 2. B737 results comparison with reference.[14].

	Elevator	Rudder	Aileron	Spoiler
Estimated hinge moment [Nm]	7600	8200	4200	3200
Reference hinge Moment [Nm]	7600	8200	4200	3800

Table 3. A320 actuators: data and results comparison.

	Elevator	Rudder	Aileron	Spoiler
Stall load [kN]	28	44	45	45
Stroke [mm]	61	109	43	84
Deflection angle []	25	25	25	50
Arm [m]	0.071	0.116	0.047	0.052
Hinge moment (stall Load·Arm) [Nm]	1990	5105	2115	2340
Hinge moment (Roskam) [Nm]	1980	5080	2100	2330

Table 4. A330 actuators: data and results comparison.

	Elevator	Rudder	Aileron	Spoiler
Estimated hinge moment [Nm]	11,700	21,400	14860/2	7230
Deduced arm [m]	0.12	0.2	0.08	0.088
Actual stall load [tons]	10.2	9.4	10	8.6
Calculated stall load [tons]	9.94	10.9	9.5	8.4

a letter in order to make it easier to trace them back from the graphs.

The surrogate model results and approaches are now shown. Each of the equations is given with their corresponding coefficient of determination (R^2). This coefficient is used on statistical models with the aim of testing hypotheses. It provides a measure of how well the outcomes are replicated by the model.

This model is limited to aircraft with a minimum MTOM of 3 tons, wing surfaces above 25 square meters, and fin surfaces bigger than 5 square meters. Also, it is meant to be used for civil subsonic aircraft since military and supersonic vehicles have different architectures and Roskam's hypothesis are not accomplished.

Ailerons

Ailerons are control surfaces used during all mission segments. The sizing condition is usually during a maneuvre at high speed since roll control has also to be guaranteed at high speed. A small deflection of the ailerons at those speeds generates huge forces on the hinge axis which are usually the highest ones in all the mission profile. For smaller aircraft with lower Mach numbers, the sizing case is sometimes during landing. The results can be seen in Figure 3. High wing surfaces result in high hinge moments. The same effect is found using the Mach number as a parameter. Both these effects can be summarized on the aircraft's maximum take-off weight for civil aircraft. Hence, the best correlation (i.e., highest coefficient of determination, R^2) was found using the MTOM as a parameter.

Equation (5) represents the correlation between aileron hinge moment and MTOM

$$M_{hinge(Ailerons)} = 0.0743 \cdot MTOM - 1679.7 \qquad (5)$$

Note that the MTOM shall be expressed in kilograms on all the following expressions, as defined in the Appendix. As explained before, heavy and light aircraft may have

Table 5. Studied aircraft.

Aircraft	Mach Cruise	MTOM (kg)	Wing Surface (m^2)	Fin Surface (m^2)
A340-300[a]	0.82	271,000	363	48
A330-300[b]	0.8	240,000	363	48
B787-8[c]	0.85	228,000	377	65.54
A300-600R[d]	0.78	171,000	260	45.5
B757-200[e]	0.8	116,000	185.3	34.37
B737-800[f]	0.75	79,000	125	26.4
A320[g]	0.78	73,500	124	21.5
ERJ190[h]	0.78	52,000	92.5	16.2
ATR90[i]	0.55	40,000	78.5	16.8
ATR72[j]	0.5	23,000	61	12.5
ATR42[k]	0.5	18,000	55	11
Cessna CJ4[l]	0.7	7761	30.66	5.4
Cessna 208[m]	0.35	3600	26	5

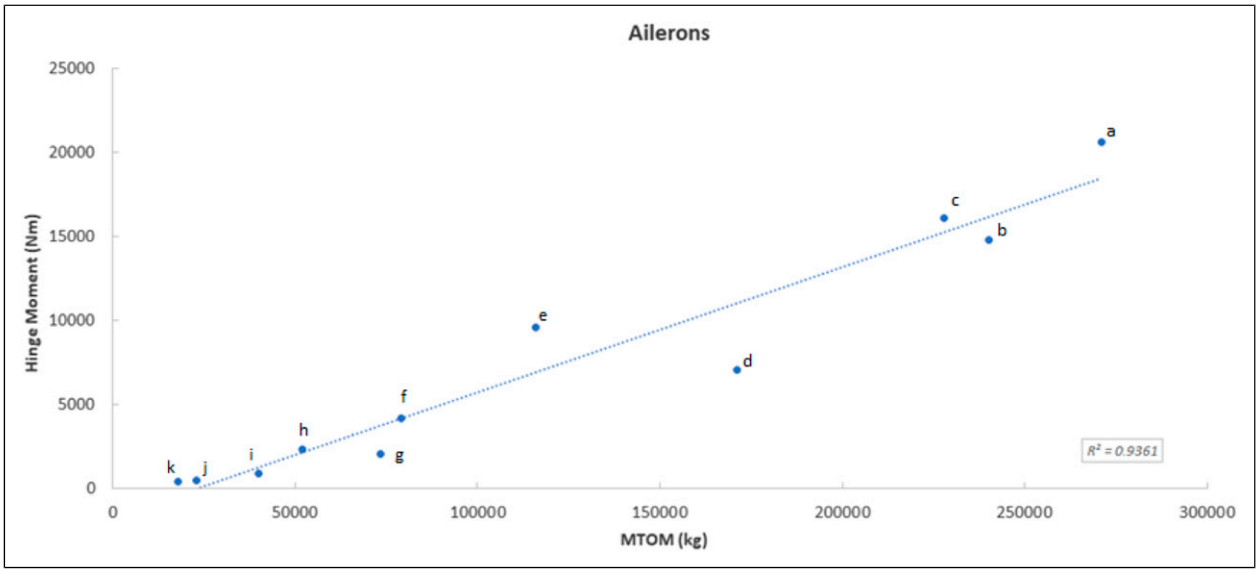

Figure 3. Surrogate model results for ailerons

different sizing cases, so the correlation is slightly different between them. In order to make a better estimation for lower-weight planes, two other equations are proposed in Figure 4.

Equation (5) is used for aircraft with MTOM bigger than 65 tons. Two other cases are defined for lighter vehicles. Equation (6) may be used for business jets. These aircraft have lower maximum take-off weight than 65 tons but still reach cruise Mach numbers close to 0.8. A better coefficient of determination is found for this approach, $R^2 = 0.987$

$$M_{hinge(Ailerons)} = 0.049 \cdot MTOM - 11.841 \quad (6)$$

Another linear regression is made for aircraft with MTOM lower than 65 tons and cruise Mach numbers lower than 0.6 (e.g., ATR 72). On these aircraft, the sizing case may not be the high speed maneuvre ,and as a result, the correlation changes. Equation (7) shows a more-accurate expression to use for light and low-speed transport aircraft. R^2 is 0.993 in this case since the sample is more bounded. For aircraft with MTOM below 3 tons, these equations should not be used since the results may be inaccurate

$$M_{hinge(Ailerons)} = 0.0244 \cdot MTOM - 30.326 \quad (7)$$

It is worth noting that this analysis provides the result for one single aileron. Bigger aircraft like A340 have two ailerons per wing side in order to reduce the wing bending moment. This equation provides the value as if there was just one aileron, so for this specific casethe value should be divided into two. Another solution is what B787 proposes. This aircraft uses one regular aileron for most of the mission profile while an extra smaller aileron, located on the middle of the wing, is used at high speeds. This allows to alleviate the wing loads, and as a result, the hinge moment is split between both ailerons.

Rudder

The rudder is analogous to the ailerons but with a main difference. While ailerons sizing scales with the wing surface, rudder sizing scales with the vertical tail surface. Still, they both have similar sizing cases on most of the situations. This results in three different equations as for the aileron case. Now, the parameter with the best correlation is the fin surface, as expected. The rudder surface itself is considered as a part of the total fin surface and should not be removed for the calculations. Results for aircraft with a take-off mass higher than 65 tons are shown in Figure 5 and equation (8) ($R^2 = 0.972$).

$$M_{hinge(Rudder)} = 546.26 \cdot S_{fin} - 5688.9 \quad (8)$$

Following the previous reasoning, two other sub-cases are analyzed for lower-weight aircraft (Figure 6). For liner transport aircraft, the best approach would be using equation (8). For small and fast transport aircraft such as business jet or a regional turbofan, then equation (9) ($R^2 = 0.972$) shall be used. For turboprop and low-speed aircraft, equation (10) ($R^2 = 0.967$) would represent the best fit. On each analysis, the equation for the most similar reference aircraft should be used. As a reference, the separation point between liner transport aircraft and smaller aircraft is suggested as MTOM which is equal to 65 tons and a fin surface of 24 square meters. For vertical tails with a surface lower than 5 square meters, this approach may fail

$$M_{hinge(Rudder)} = 368.11 \cdot S_{fin} - 1420.1 \quad (9)$$

$$M_{hinge(Rudder)} = 203.94 \cdot S_{fin} - 1059.6 \quad (10)$$

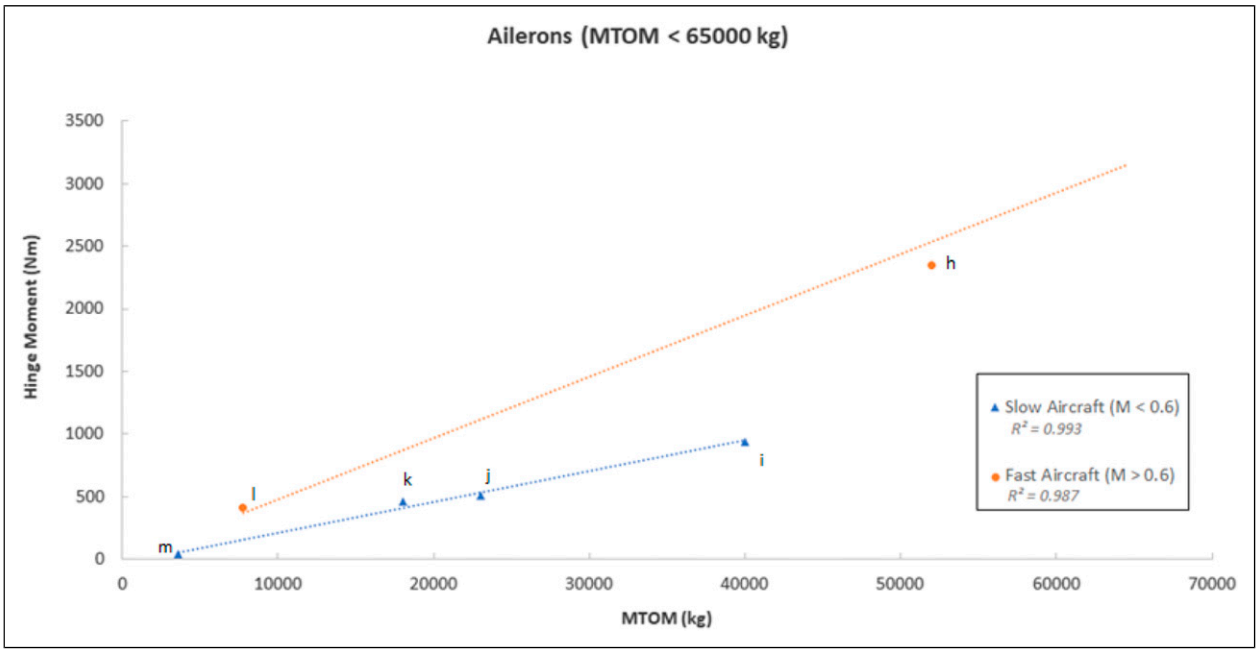

Figure 4. Surrogate model results for ailerons for smaller aircraft

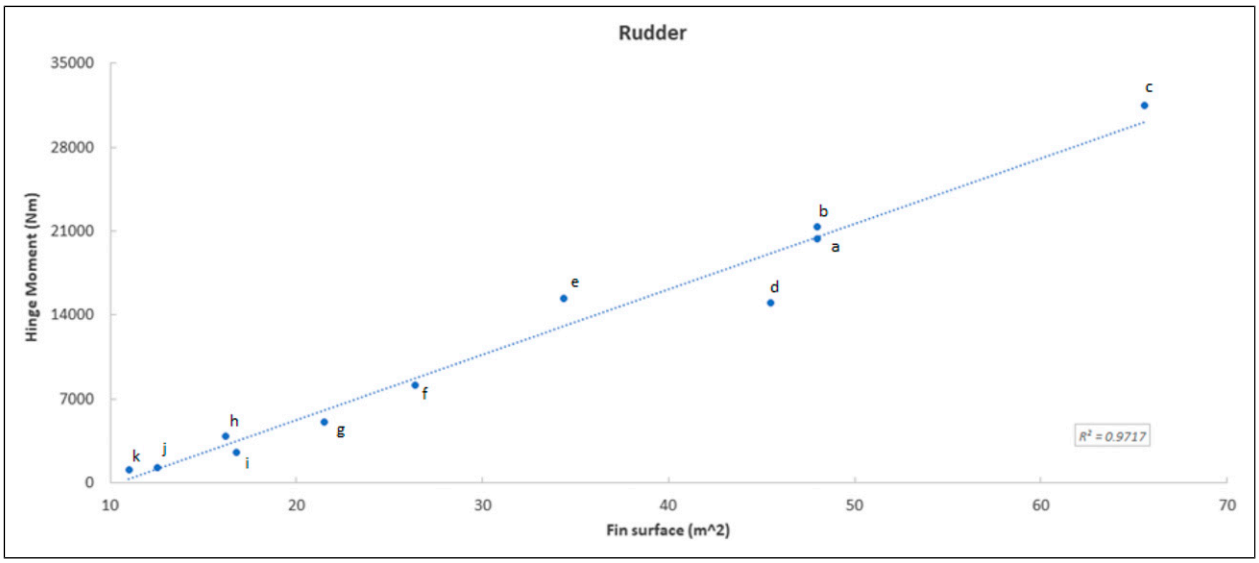

Figure 5. Surrogate model results for rudder

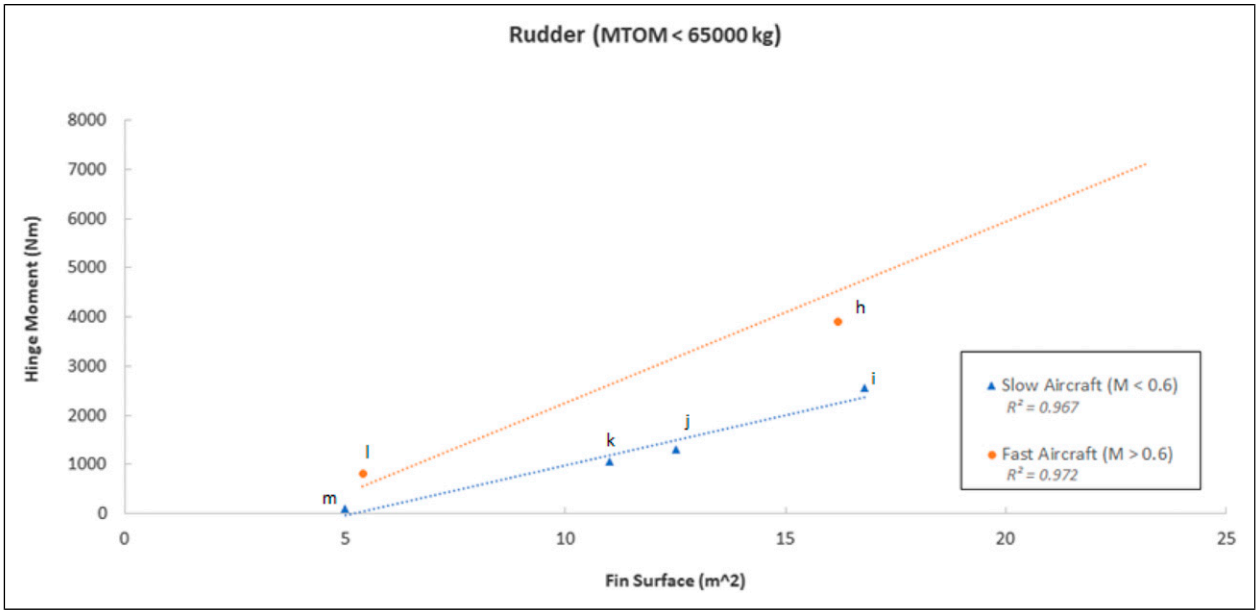

Figure 6. Surrogate model results for rudder for smaller aircraft

Elevator

Although elevator can be seen as an analogous case to the ailerons, this assumption is not correct. Even though they have similar sizing cases and are referred to similar surfaces, results show a huge non-linearity. While the variables with the highest impact on the ailerons' hinge moment were the wing surface and Mach number, more parameters highly affect the elevator. A correlation with the horizontal tail plane surface was not found. The most-accurate approach is shown in Figure 7 where the hinge moment for the elevator is correlated with the aircraft MTOM. Two different tendencies are seen. Bigger aircraft have much higher hinge moment values than lower ones, both tending to two different values. While on the middle, for aircraft with MTOM close to 70 tons, values may highly vary. This variation may be explained due to the effect of the trimmable horizontal stabilizer (THS) angle. Depending on this angle, the results may differ considerably. The result is shown on equation (11) ($R^2 = 0.931$). For MTOM > 250 tons, this equation should not be used and a deeper analysis shall be done. If not possible a reference value of 12,000 Nm is suggested

$$\mathrm{M}_{hinge(Elevator)} = 652.1 - 1.3212 \cdot 10^{-22} \cdot MTOM^5 + 1.0912 \cdot 10^{-16} \cdot MTOM^4 - 3.2663 \cdot 10^{-11} \cdot MTOM^3 + 3.9390 \cdot 10^{-6} \cdot MTOM^2 - 8.7733 \cdot 10^{-2} \cdot MTOM \quad (11)$$

For smaller aircraft, the effect of the THS is negligible. Another equation focused on these cases is provided,

equation (12) ($R^2 = 0.998$). This approach may be used for MTOM ≤56.5 tons. And provides more reliable values as seen on the coefficient of determination value. The equation is also represented in Figure 8

$$M_{hinge(Elevator)} = -128.6 + 8.3793 \cdot 10^{-11} \cdot MTOM^3 - 5.2471 \cdot 10^{-6} \cdot MTOM^2 + 9.9849 \cdot 10^{-2} \cdot MTOM \quad (12)$$

Spoilers

Spoilers' moments have a clear correlation with the wing surface. These devices are deployed during landing to break lift and generate drag. The bigger the aircraft, the bigger the total spoiler surface needs to be. Results are shown in Figure 9 and in equation (13) ($R^2 = 0.960$). Only ground spoilers are considered, as explained in previous sections. Values for flight spoilers are supposed to be similar to ground spoilers

$$M_{hinge(Spoilers)} = 20.828 \cdot S_{wing} - 235.32 \quad (13)$$

As in the previous cases, for smaller aircraft, the approach can be improved by just analyzing the relevant cases (Figure 10). For aircraft with 65 tons of MTOM or less, two other equations are proposed. Aircraft with a cruise Mach number higher than 0.6 should be modeled

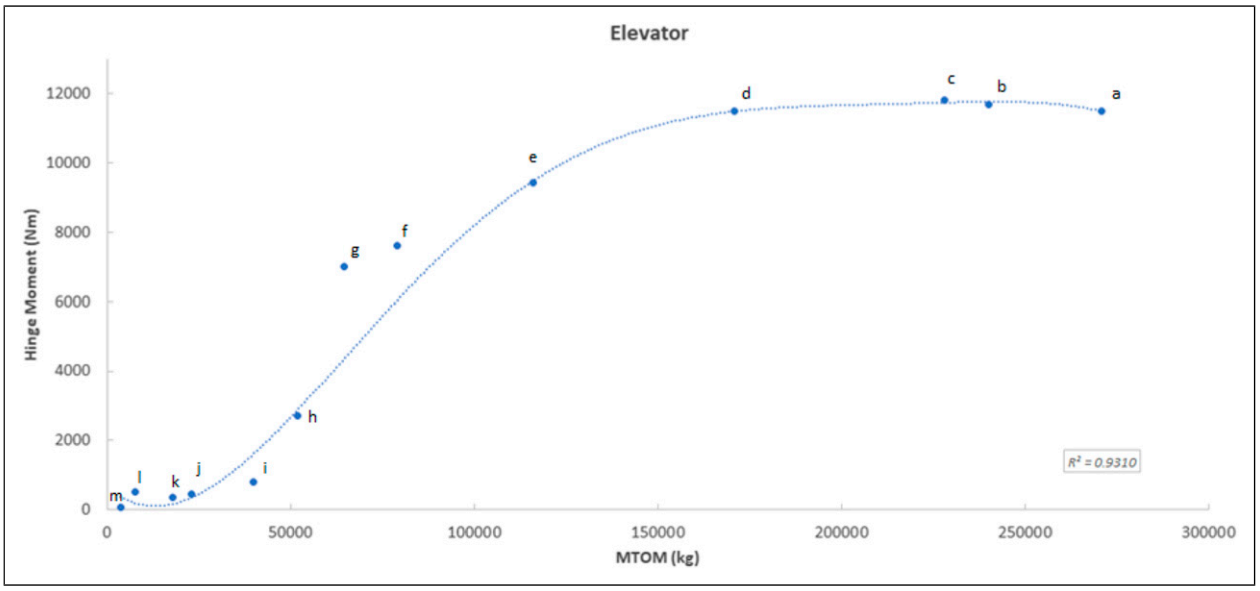

Figure 7. Surrogate model results for elevator

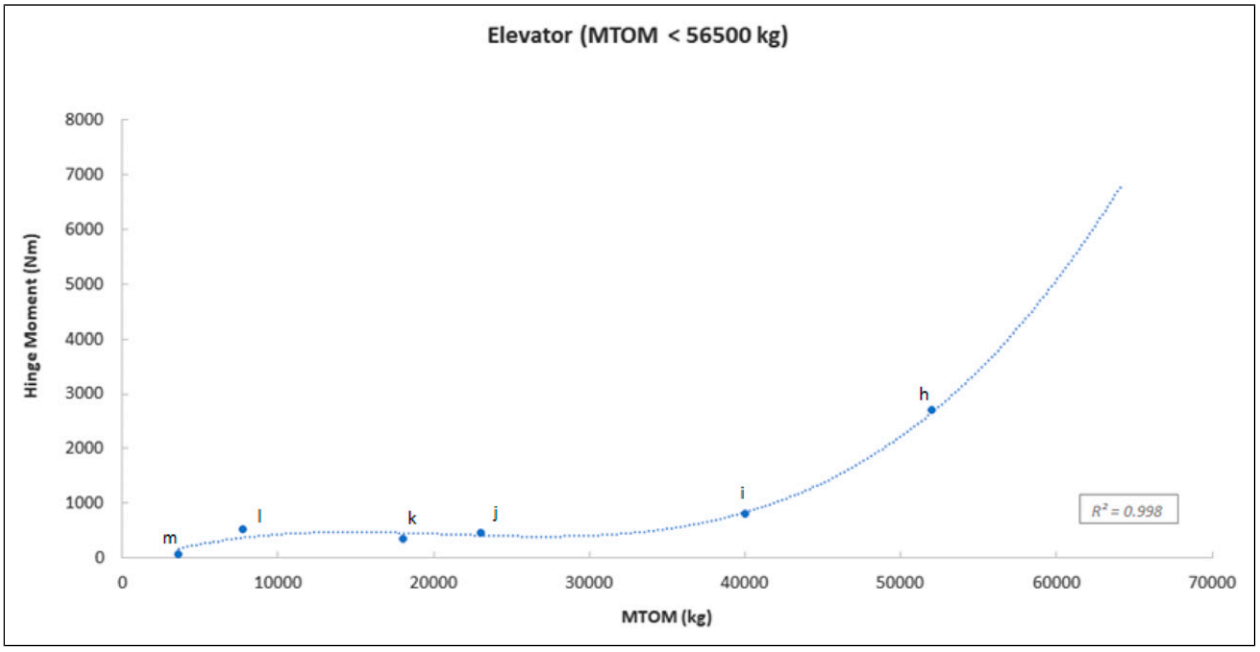

Figure 8. Surrogate model results for elevator for smaller aircraft

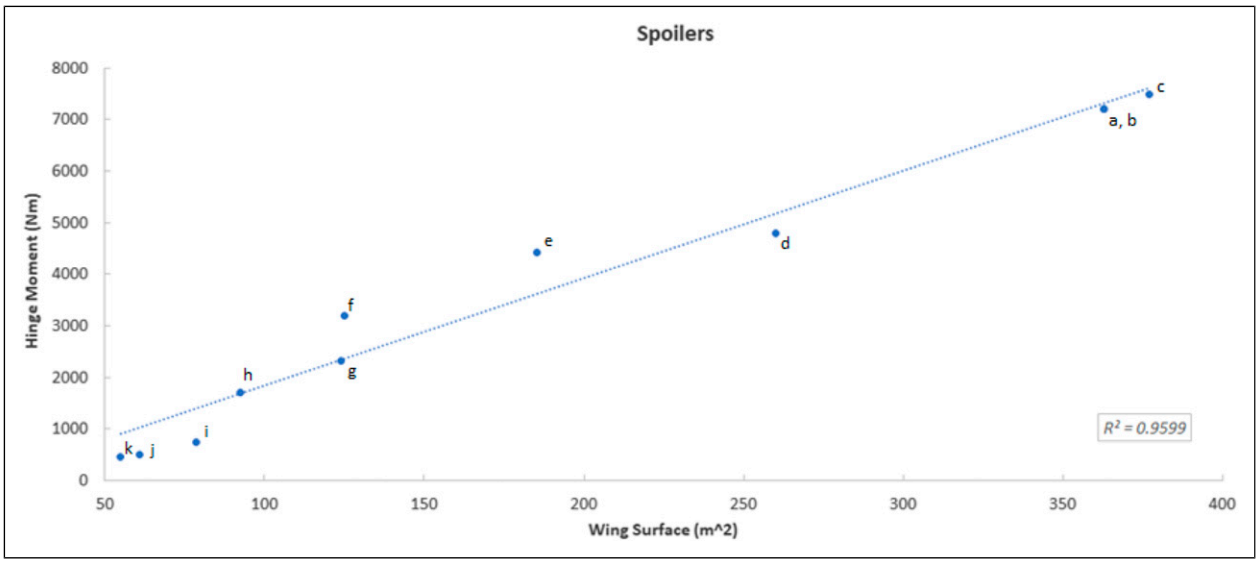

Figure 9. Surrogate model results for spoilers

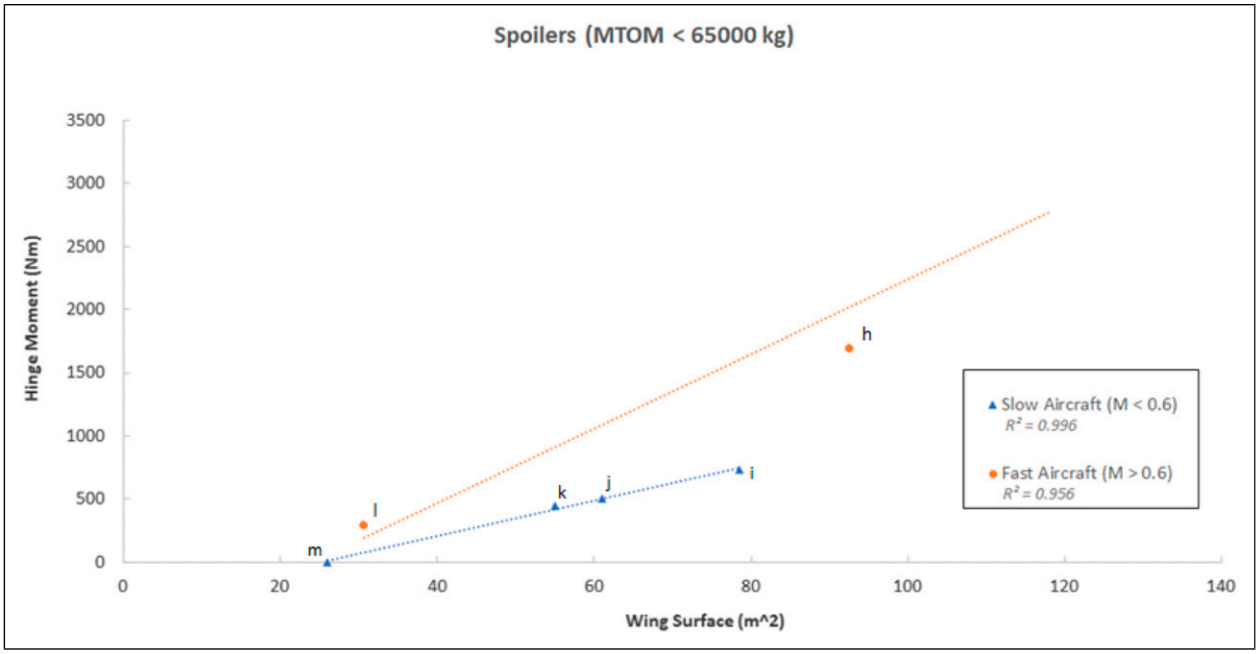

Figure 10. Surrogate model results for spoilers for smaller aircraft

with equation (14) (R^2 = 0.956) while those ones with a lower Mach number are better estimated with equation (15) (R^2 = 0.996). The surrogate model should not be used for aircraft with a wing surface lower than 25 square meters

$$M_{hinge(Spoilers)} = 29.5 \cdot S_{wing} - 708.11 \quad (14)$$

$$M_{hinge(Spoilers)} = 14.037 \cdot S_{wing} - 352.55 \quad (15)$$

Flaps

As explained in previous sections, flaps are sized by a force and not by a hinge moment. Flaps are only active during take-off and landing. In most of the cases, the sizing case is during landing since the speed and the deflections are higher. In this case, the correlation with the wing surface is expected and found. Figure 11 shows it and equation (16) (R^2 = 0.9926) can be used for the estimation

$$F_{Acts(Flaps)} = 541.8 \cdot S_{wing} - 3832.6 \quad (16)$$

In this case, since flaps are sized during landing and not on cruise, there is no need of dividing aircraft into high-speed and low-speed ones. This value then shall be divided by the number of flap actuators to calculate their stall load. The A320 is now explained as an example for the reader. Two in-board and two out-board flaps are found

in the A320, each of them has two actuators attached, reaching a total number of 8 actuators. Hence, the flap ball-screw-single-actuator stall load required for this aircraft is obtained by just taking the value found with equation (16) and dividing it by 8.

Slats

Flaps and slats are completely analogous. Both are sized during landing or take-off and are referred to the same wing surface. The results are structured in the same way. Figure 12 shows the linear regression, and equation (17) ($R^2 = 0.9877$) may be used for the estimation

$$F_{Acts(Slats)} = 337.25 \cdot S_{wing} - 1881.1 \quad (17)$$

It is worth noting that aircraft with MTOM lower than 30 tons do not usually have slats, but in case they have, the surrogate model can still be used. An example on how to interpret these results is now provided. A320 has four outboard slats and one in-board one. This makes a total of ten slats with two actuators per control surface. Dividing the value found in equation (17) by that in equation (20) gives the average-slat-actuator stall load. It can be realized that this analysis provides with a global value; if different slats are used on the same aircraft, the result shall be split into them, so it allows to calculate different architectures.

Mass and power estimation

The actuators can be sized once the hinge moment has been estimated. With the surrogate model, the hinge model for spoilers, ailerons, elevator, and rudder are calculated. The actuator stall load can be obtained after estimating the arm of the hinge moment. Hence, the mass of each

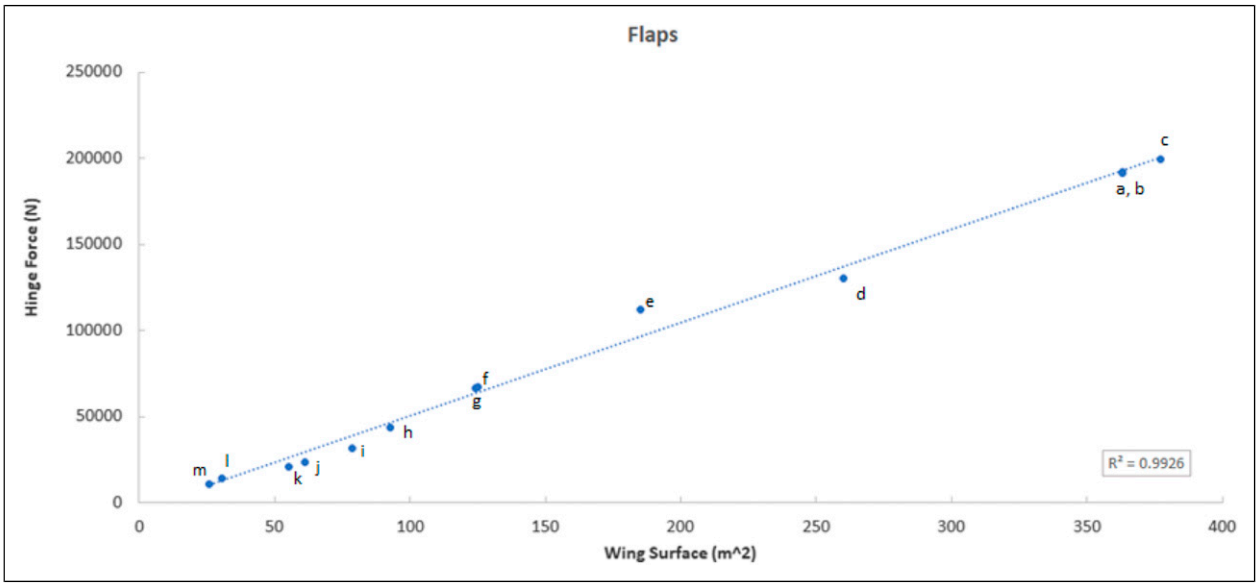

Figure 11. Surrogate model results for flaps

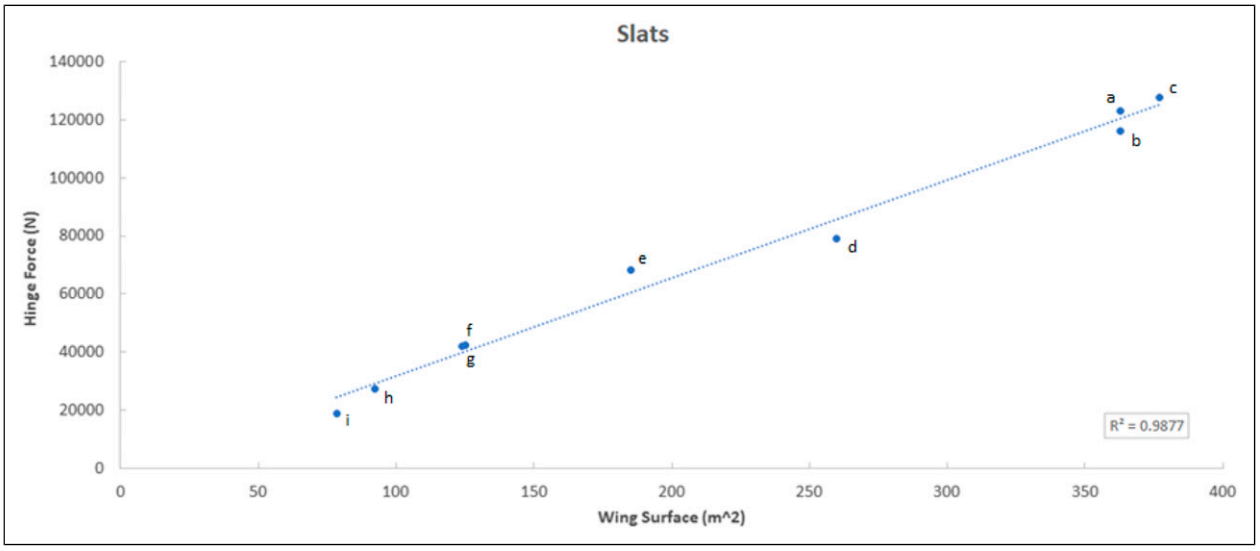

Figure 12. Surrogate model results for slats

actuator can now be estimated. The actuator load for the high lift devices is already known from the surrogate model. In this case, the mass of the actuators is calculated and also the mass contribution associated to the shafts, gearboxes, torque limiters, and power drive units (PDU).

Ailerons, elevator, rudder, and spoilers

The hinge moment for these control surfaces has been estimated in the previous section. Estimation for the arm of the moment is now needed. The estimation for the arms of the actuators of the A320 was done in the section Model Calibration, the results obtained provided good results. In order to estimate the arm or different aircraft, a proportion with the wing chord is suggested. Hence, the arm for another aircraft would be the A320 reference value multiplied by a factor. This factor is the division between the wing chords of both aircraft. With the hinge moment and arm values, the stall load for each of the actuators is obtained.

The mass of an actuator grows with the power that it needs to provide. A linear regression with the stall load is proposed. This approximation is made with values from database and are consistent with other similar studies.[20] Equation (18) shows the mass estimation for a conventional hydraulic actuator

$$Mass_{HSA} = 0.001951 \cdot SL_{Actuator} + 0.6243 \tag{18}$$

The mass of an EHA and EMA is higher if compared to a classic hydraulic actuator. Some analyses are performed on this topic,[3,20] and a simplified model is proposed. The EHA mass can be between 1.5 and 1.8 times more than the classic hydraulic one for the common aircraft, as shown in some analyses.[3] Hence, the EHA mass is calculated with the result from equation (18), and then multiplying it by a suggested average factor of 1.6. Regarding the EMA, the mass can be approximated by the one obtained for an EHA multiplied by another factor. This factor can be 0.5 for small aircraft, 0.9 for A320-like aircraft, and even higher than 1 for bigger aircraft.[3] For general cases, a factor of 0.9 is suggested. It is worth noticing that the heaviest actuator is usually the EHA.

The maximum power required by each actuator can now be estimated with equation (19). This equation can be obtained by deriving the equation that represents the power required by the actuator during its deployment and finding the maximum point[25]

$$Power_{act} = \frac{2}{3} \cdot M_{hinge} \cdot \frac{1}{\sqrt{3}} \cdot w_{surface} \tag{19}$$

Flaps and slats

The stall load for flaps and slats is known directly from the surrogate model. The methodology is the same for both cases. A reference flap drive system architecture is shown in Figure 13 for a better understanding of the model. It is worth noticing that "GB" stands for gearbox and "TL" for torque limiter.

The first step to estimate the mass for all the flap devices is to divide the force obtained from the surrogate model by the number of actuators. In Figure 13, for instance, two in-board and two out-board flaps are shown (one of each per wing, only one semi-wing is represented in the figure). There are two actuators per flap, making a total of eight actuators. If a more precise estimation is wanted, equation (4) can be used for each flap and then divided by the number of actuators for that flap. This allows to estimate the stall load for each actuator instead of having an average value of all of them.

The required force for the flap actuators is now known. A classic linear ball-screw actuator is suggested to be used for this analysis. These actuators provide a force when a torque is given as input.[26] Equation (20) shows the relation between the input torque and the output stall load

$$T_{bs} = \frac{lead_{bs} \cdot SF_{Actuator}}{2 \cdot \pi \cdot \eta_{bs}} \tag{20}$$

where 2 mm is suggested as a typical value for the $lead_{bs}$[22] and 0.75 for the efficiency η_{bs}. The efficiency value is low since the actuator works at freezing temperatures and the friction can deteriorate its performance.[22]

Following the schema proposed in Figure 13, the torque required by each actuator is now known. The input torque for each gearbox is the output torque divided by an efficiency value that is usually 0.85 for corner gearboxes or 0.9 for the PDU gearbox.[22] The required PDU torque is sized by summing all the torques. A torque limiter is usually positioned at the end of the drive system to avoid overloads.

The shafts should also be sized. Each transmits the torque between gearboxes. This torque is now known and by choosing a material the shafts can be properly defined. Equation (21) shows how to calculate the shaft radius

$$r_{shaft} = \sqrt[3]{\frac{2 \cdot Torque}{\pi \cdot \tau}} \tag{21}$$

where *Torque* is the corresponding torque for each tube multiplied by a safety factor of 1.5 and τ is the maximum allowable shear stress, which is 270 MPa for an aluminum 6061-T6 alloy. With the radius and the material density, the mass of each shaft is easily obtained.

The screw-jack and PDU mass estimation can be found in Ref.27. They are both obtained from the torque value. For the gearboxes and torque limiters, another reference is provided.[23] All these masses can now be estimated since the torques are known. The reference values for the A320 are provided in the section Application Case: A320 FCS Mass Estimation. The flap support structure (i.e., support and moving bars) is not included since it is a part of the wing's mass.

This mass estimation method allows to know the mass on a component level. The method is more precise than other general ones that simply estimate the overall FCS mass as a proportion of the MTOM or wing surface.

Slats mass estimation is carried out in an analogous way. The number of actuators per slat is also two, and each ball-screw actuator is connected to a 90-degree gearbox. The respective torques are summed, dividing by each gearbox efficiency. All the efficiency values are the same as for the flaps. The slat PDU is hence sized the same way as for the flaps.

An estimation for the PDU rotation speed is needed in order to estimate the power required by the drive system. The maximum power required by flaps and slats can be obtained using equation (22). The global torque is obtained by summing the torque required by left and right wings, that was calculated before by summing the actuator torques and dividing by the corresponding efficiencies. The rotation speed can be estimated knowing the flaps and slats excursion times. The linear speed requirement for the actuator can be transformed into a rotary speed for the drive system shafts since the stroke and lead of the ball-screw are known. All the gearboxes have a relation of 1:1 so the PDU rotation speed is the same as the shafts rotation speed. The higher rotation speeds are usually found on the first period of the flap mechanisms deployment,[22] so the maximum power required for the flaps can be found during this period

$$Power_{PDU} = Torque_{PDU} \cdot w_{PDU}\sqrt{2} \tag{22}$$

The FCS power requirement can be obtained by summing the results for each actuator, flaps PDU, and slats PDU. This analysis has to be done per mission segment, specifying which control surface is active on each segment. Hence, the results show the power required by the FCS on each mission segment, and the maximum and average values can then be calculated so that the system is properly sized.

Application case: A320 FCS mass estimation

An application case is now shown. The scope of it is comparing this new methodology to previous existing ones to check the reliability of the model. First, the hinge moments were estimated with the surrogate model. Then, the mass of each actuator was calculated. Finally, the flap and slat devices were sized, and their mass was summed to have a global value for the whole FCS.

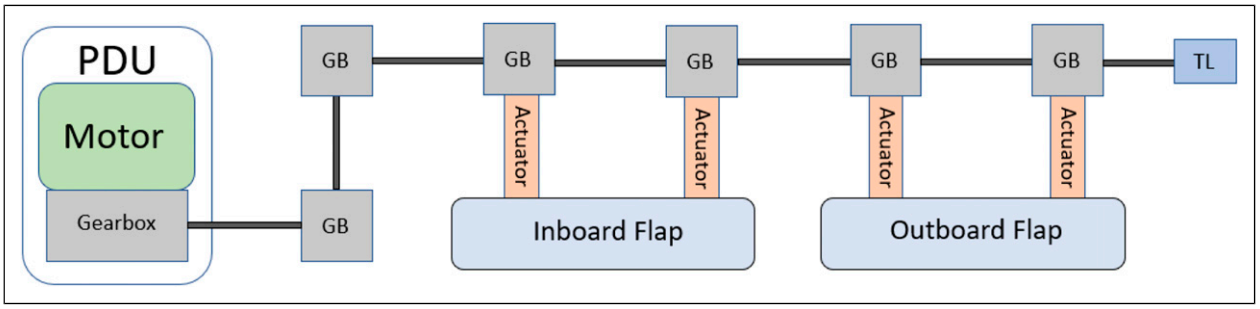

Figure 13. Flap drive system distribution example

Table 6. A320 estimated FCS components mass.

Component	Number of components	Mass of one component (kg)
Aileron actuator	4	9.6
Elevator actuator	4	6.2
Rudder actuator	3	9.4
Spoiler actuator	10	9.6
Flap ball-screw actuator	8	13
Flap gearbox	8	12
Flap corner gearbox	4	13.3
Flap torque limiter	2	5.5
Flap PDU	1	57.7
Flap tubes	all tubes	3.7
Slat ball-screw actuator	20	3.35
Slat gearbox	20	6.14
Slat corner gearbox	2	6.7
Slat torque limiter	2	2.8
Slat PDU	1	29.1
Slat tubes	all tubes	2.6
Total	-	**756**

756 is the exact value summing the previous components with all the decimals. Since the previous components have been rounded in the table, the summ is a bit less. Significance would be 2.5 kg or 0.33%.

Table 7. A320 FCS mass comparison among methods.

Method	FCS mass (kg)
Raymer	575
Torenbeek	1037
Beltramo	805
New method	756

The new proposed method is able to estimate the mass of each of the FCS components providing a more reliable result than other statistical methods that just provide an overall result for the whole subsystem. The new methodology can also be very useful for on-board systems integration when the mass and position of each component is needed. Component-level results for the A320 are shown in Table 6. It is worth noticing that the A320 uses hydraulic actuators for all the control surfaces.

A comparison with other methods is now shown. Results are provided in Table 7. Raymer proposes an FCS mass estimation method based on some top-level aircraft requirements. He makes a differentiation among several aircraft types (e.g., business jets and regional turboprop) and provides a statistical formula for each of them based on different parameters.[28] Torenbeek[29] also proposes a statistical regression for different aircraft types depending on the aircraft maximum take-off mass. Beltramo's method is based also on statistical data; he uses the surfaces of the wing, horizontal and vertical tails for the analysis, having a more precise result since it is based on the actual control surfaces area.[30]

Conclusions

A new methodology for flight control system design on early design stages is proposed. The need for it resides mostly when comparing different architectures. One example is the current tendency moving towards more-electric aircraft where new actuators are used and hydraulic lines are progressively being removed. The FCS impact on the aircraft weight can now be estimated with this methodology making it possible to compare the results between the old and new trends.

The need for an input reduction has been highlighted, and a surrogate model for hinge moment estimation is provided. Each control surface has been analyzed with the most appropriate method possible during preliminary design. Roskam's method is implemented for ailerons, rudder, and elevator. The flat plate model is used for the spoilers. Normal load calculation analysis is performed for flaps and slats.

The results from the surrogate model are provided. Thirteen aircraft from different sizes were used in order to have an appropriate amount of data properly spaced on the design space. The linear correlations are done with top-level aircraft requirements, which are, in this case, the MTOM, wing surface, and fin surface. This allows to use the method on early stages of the project, as wanted.

The results from the hinge moment surrogate model are used for the mass estimation. The analysis differentiates ailerons, rudder, elevator, and spoilers from flaps and slats. The mass of each actuator of each control surface is estimated as well as all the flap and slat devices between the actuator and the PDU that are needed for their deployment.

An application case based on the A320 is shown to validate the model comparing it to other classic ones. This new methodology provides component-level data making it possible to make systems installation and mass distribution analysis during preliminary design unlike the other methods.

Declaration of conflicting interests

The author(s) declared no potential conflicts of interest with respect to the research, authorship, and/or publication of this article.

Funding

The author(s) received no financial support for the research, authorship, and/or publication of this article.

ORCID iDs

Carlos Cabaleiro de la Hoz https://orcid.org/0000-0003-3964-8405
Marco Fioriti https://orcid.org/0000-0003-2762-1088

References

1. Cronin MJ. All-electric vs conventional aircraft – The production/operational aspects. *J Aircr* 1983; 20(6): 481–486.
2. Sinnett M. 787 no-bleed systems: saving fuel and enhancing operational efficiencies. *Aero Q* 2007; 18: 6–11.
3. Vladimirov S and Forde S. Demonstration program to design, manufacture and test an autonomous electro-hydrostatic actuator to gimbal large booster-class engines. In: 42nd AIAA/ASME/SAE/ASEE joint propulsion conference & exhibit, Sacramento, CA, 09–12 July 2006.
4. Chakraborty I and Mavris DN. Integrated assessment of aircraft and novel subsystem architectures in early design. *J Aircr* 2017; 54(4): 1268–1282.
5. Qiao G, Liu G, Shi Z, et al. A review of electromechanical actuators for more/all electric aircraft systems. *Proc Inst Mech Eng J Mech Eng Sci* 2018; 232(22): 4128–4151.
6. Rongjie K, Zongxia J, Shaoping W, et al. Design and simulation of electro-hydrostatic actuator with a built-in power regulator. *Chin J Aeronaut* 2009; 22(6): 700–706.
7. S Airbus SA. *Airbus Training - A320 Flight Crew Operating Manual: Flight Controls*. Phoenix Simulations Software. 23 February, 2002.
8. Le Tron X. *A380 Flight Controls Overview. Presentation at Hamburg*. Hamburg: University of Applied Science, September 2007, p. 27.
9. S Airbus SA. *Airbus Training – A350-900 Flight Deck and Systems Briefing for Pilots*. Issue 02, Sept 2011.
10. Corcione S. *Analisi numerica del momento di cerniera di superfici aerodinamiche di controllo. Università degli Studi di Napoli Federico II*. 2011.

11. Roskam J. *Airplane Design Part vi: Preliminary Calculation of Aerodynamic, Thrust and Power Characteristics*. Lawrence, Kansas, USA: DAR corporation, 2000.
12. Xue L. *Actuation Technology for Flight Control System on Civil Aircraft*. PhD thesis. Cranfield, England: Cranfield University, 2009.
13. Meng F. *Actuation System Design with Electrically Powered Actuators*. PhD thesis. Cranfield, England: Cranfield University, 2011.
14. Chakraborty I, Mavris DN, Emeneth M, et al. A system and mission level analysis of electrically actuated flight control surfaces using Pacelab SysArc. In: 52nd aerospace sciences meeting, National Harbor, Maryland, 13-17 January 2014, p. 381.
15. Behrens T and Zhu WJ. Feasibility of aerodynamic flap hinge moment measurements as input for load alleviation control. In: European Wind Energy Conference and Exhibition 2011. pp. 28–32.
16. Kelly JA and McCullough GB. *Aerodynamic Loads on a Leading-Edge Flap and a Leading-Edge Slat on the naca 64a010 Airfoil Section*. USA: National Advisory Committee for Aeronautics, 1954: 3220.
17. Fry EB. *Flight Measurements of Hinged-Plate Wing-spoiler Hinge Moments*. Ames Research Center: National Aeronautics and Space Administration, 1983.
18. Harley CD and Crowther B. *Aerodynamic Performance of Low Form Factor Spoilers*. Manchester, England: University of Manchester, 2010.
19. Taira K and Colonius T. Three-dimensional flows around low-aspect-ratio flat-plate wings at low Reynold's numbers. *J Fluid Mech* 2009; 623: 187.
20. Chakraborty I, Mavris DN, Emeneth M, et al. A methodology for vehicle and mission level comparison of more electric aircraft subsystem solutions: application to the flight control actuation system. *Proc Inst Mech Eng J Mech Eng Sci* 2015; 229(6): 1088–1102.
21. Li J, Yu Z, Huang Y, et al. A review of electromechanical actuation system for more electric aircraft. IEEE International Conference on Aircraft Utility Systems (AUS), Beijing, China, 10-12 October 2016. IEEE, pp. 490–497.
22. Ghimire A. *Power Sizing Approaches and Methods for Trailing Edge High Lift Control Devices during Preliminary Phase of Aircraft Development*. PhD thesis. Wichita, KS, USA: Wichita State University, 2019.
23. Zaccai D, Bertels F and Vos R. Design methodology for trailing-edge high-lift mechanisms. *CEAS Aeronaut JournalSpringer* 2016; 7(4): 521–534.
24. Rudolph PKC. *Mechanical Design of High Lift Systems for High Aspect Ratio Swept Wings*. Ames Research Center: National Aeronautics and Space Administration, 1998.
25. Maré JC. *Aerospace Actuators 1: Needs, Reliability and Hydraulic Power Solutions*. Hoboken, NJ, USA: John Wiley & Sons, 2016.
26. Shigley JE, Mischke CR and Budynas RG. *Mechanical Engineering Design*. Chapter 7. Newyork: Mc Grawhill, 2001.
27. Budinger M. *Preliminary Design and Sizing of Actuation Systems*. UPS Toulouse, 2014.
28. Raymer D. *Aircraft Design: A Conceptual Approach*. Reston, VA, USA: American Institute of Aeronautics and Astronautics, Inc, 2012.
29. Torenbeek E. *Advanced Aircraft Design: Conceptual Design, Analysis and Optimization of Subsonic Civil Airplanes*. Hoboken, NJ, USA: John Wiley & Sons, 2013.
30. Beltramo MN, Morris MA and Anderson JL. Application of Parametric Weight and Cost Estimating Relationships to Future Transport Aircraft. Proceeding of 38th Anual Conference of SAWE, New York, USA, 7–10 May 1979.

Appendix

Notation

$arm_{spoiler}$	Spoiler Actuator Arm $[m]$
c	Standard Mean Chord $[m]$
$C_{d_{spoiler}}$	Spoiler Drag Coefficient $[\ -\ ]$
C_h	Hinge Moment Coefficient $[\ -\ ]$
$C_{N_{flap}}$	Normal Flap Load Coefficient $[\ -\ ]$
c_f	Plain Flap Chord $[m]$
$c_{spoiler}$	Spoiler Chord $[m]$
CFD	Computational Fluid Dynamics
δ	Control Surface Deflection [°]
$EBHA$	Electric Backup Hydraulic Actuator
EHA	Electro-Hydrostatic Actuator
EMA	Electro-Mechanical Actuator
F_{Acts}	Actuators Force $[N]$
FCS	Flight Control System
HSA	Conventional Hydraulic Servo Actuator
$lead_{bs}$	Lead of a Ball-Screw Actuator $[m]$
$Mass_{HSA}$	Mass of a HSA $[kg]$
MEA	More Electric Aircraft
M_{hinge}	Hinge Moment $[Nm]$
$MTOM$	Maximum Take-Off Mass $[kg]$
N_f	Normal Flap Load $[N]$
η_{bs}	Efficiency of a Ball-Screw Actuator $[\ -\ ]$
PDU	Power Drive Unit
$Power_{act}$	Power Required by the Actuator $[W]$
q	Dynamic Pressure $[Pa]$
R^2	Coefficient of Determination $[\ -\ ]$
r_{shaft}	Shaft radius $[m]$
$SL_{Actuator}$	Actuator Stall Load $[kg]$
$SF_{Actuator}$	Actuator Stall Force $[N]$
S_{wing}	Wing Surface $[m^2]$
S_{fin}	Fin Surface $[m^2]$
S_{flap}	Flap Surface $[m^2]$
$S_{spoiler}$	Spoiler Surface $[m^2]$
τ	Maximum Allowable Shear Stress $[Pa]$
THS	Trimmable Horizontal Stabilizer
T_{bs}	Torque of a Ball-Screw Actuator $[Nm]$
$w_{surface}$	Excursion Speed $[rad/s]$